5. A review of synthesis of nanoparticles in the gas phase for electronic, optical and magnetic applications

In the preceding chapters the applications of nanoparticles, the synthesis methods and the relevant mechanisms were described. In this chapter most of the relevant works are described which are done using gas-phase methods to obtain nanoparticles or nanoparticle-based films and powders for electronic, optical and magnetic applications. Parts of this review have been published (Kruis *et al.*, 1998d). This background allows to choose two interesting functional applications. The requirements for a process suitable for complying with the requirements for these applications will be discussed, finally leading to the selection of a synthesis process.

5.1. Synthesis for microelectronic and optoelectronic applications of zero-dimensional structures (quantum dots)

Synthesis of semiconducting nanoparticles was pioneered by Kaito *et al.* (1976), who evaporated CdS powder from a boat heated at 1100°C in a low-pressure inert gas. The particles, ranging from 10 to 100 nm, were collected on TEM grids at various positions in the produced aerosol. The same procedure was also applied by Kaito *et al.* (1983) to CdTe. Agata *et al.* (1990) synthesized CdS nanoparticles of 20-150 nm by evaporating CdS powder in low-pressure Ar. However, quantum effects were not detected in the photoluminescent spectra due to the relatively large size of the particles. Nevertheless the photoluminescence intensities increased with decreasing particle size, probably related to the appearance of new electronic states on the free surface. Hayashi *et al.* (1989) detected quantum effects in gas-evaporated ZnTe nanoparticles with sizes between 20 and 80 nm by measuring the Raman spectrum. The change in the relative intensities of the different Raman lines indicated a blue shift of the ground-state energy. In order to avoid problems due to incongruent evaporation, Kaito and Saito (1990) co-evaporated the metals (Zn, Cd) and the chalcogenides (S, Se, Te) from two boats kept at different temperatures. Thus the vapor pressures of both elements could be matched and several II-VI semiconductor nanoparticles compounds were obtained.

Saunders *et al.* (1992) synthesized semiconductor nanoparticles from the gas phase in order to obtain quantum confinement effects. GaAs nanoparticles in the 5-10

nm size range were formed from the nonequilibrium vapor created by the exploding wire method. Optical extinction measurements of the nanoparticles when collected in a liquid were suggestive of quantum size effects, especially due to the fact that a distinct absorption edge at the bulk material band gap was absent. Sercel *et al.* (1992) obtained GaAs nanoparticles by using an organometallic precursor. $(CH_3)_3Ga$ was mixed in a furnace flow reactor with AsH_3 gas yielding crystalline GaAs particles with sizes between 10 and 20 nm. Saunders *et al*. (1993b) showed that when $(CH_3)_3Ga$ was pyrolyzed to form Ga nanoparticles, the GaAs nanoparticles obtained after the addition of AsH_3 had a different morphology as compared to the case where $(CH_3)_3Ga$ and AsH_3 were premixed. In the premixed case, homogeneous nucleation of GaAs clusters was probably the dominant mechanism. The optical absorption spectrum showed in this case quantum confinement effects.

As the quantum confinement effect is a sensitive function of particle size (Yoffe, 1993), a narrow size distribution is required to observe it experimentally otherwise the size effect will be averaged out. To this end, a differential mobility analyzer (DMA) can be used to 'size-select' an aerosol at atmospheric pressure (Fissan *et al.*, 1996). An indirect way to obtain quantum dot structures is by depositing size-selected metallic aerosol particles onto InP wafers. After etching away the uncovered surface of the wafer, free-standing columns of semiconducting material result (Wiedensohler *et al.*, 1992; Stratmann *et al.*, 1993; Deppert *et al.*, 1994). The diameter of these columns, between 20 and 50 nm, was defined by the size of the masking aerosol particles. The height of these columns, typically 150 nm, is dependent on the etching time. Maximov *et al.* (1993) measured cathodoluminesence of the created quantum dot structures and obtained a blue shift in the luminescence peak, although this effect could not be explained by confinement effects alone. A similar etching method was used by Kim and Rye (1994) to obtain GaAs quantum dots by reactive ion etching of a GaAs wafer covered with SiO_2 nanoparticles. These particles were synthesized by electrospraying a TEOS solution in ethanol in an O_2 atmosphere.

Size-selected quantum dots can also be produced directly. Deppert *et al.* (1996) evaporated Ga in a furnace flow reactor and then size-selected the formed Ga nanoparticles. Finally, by adding AsH_3 gas in a second furnace, the Ga nanoparticles were reacted to obtain GaAs nanoparticles. This complicated route was used because GaAs does not evaporate stoichiometrically. Kruis *et al.* (1996) on the other hand showed that PbS, which belongs to the group of IV-VI semiconductors, can be directly sublimated in a furnace flow reactor without decomposition. This yielded amorphous PbS nanoparticles which were then size-selected. Control over particle deposition was obtained by creating a lateral electric field between the electrodes, resulting in the particles depositing preferentially on one electrode. Another method uses photoresist

patterns on the substrate. The particles deposit preferentially on the areas without photoresist, probably due to charging of the photoresist. The photoresist is removed afterwards without visible loss of particles. As a first device application metal-semiconductor-metal photodetectors with multifinger interdigitated electrodes were produced. After nanoparticles deposition the detectors show a higher sensitivity, 4x on a GaAs substrate and 60x on a Si substrate (Prost *et al.*, 1998).

Koyama *et al.* (1992) used laser ablation to obtain CdS and CdTe nanoparticles with stoichiometric composition. Substrates placed in a low-pressure chamber were ablated using a pulsed Nd:YAG laser. The nanoparticles formed were transported through a pipe into a vacuum collection chamber where they deposited onto a cold finger and were covered with frozen methanol. The nanoparticle diameter could be controlled between 4 and 10 nm by changing the laser power and the inert gas pressure. Absorption spectra indicated quantum size effects. Using the same experimental setup, a glass doped with CdTe microcrystallites was produced by ablating alternatively a CdTe target and a SiO target in an O_2 atmosphere (Ohtsuka *et al.*, 1992). In this case, nanoparticles with nonlinear optical properties were obtained.

Danek *et al.* (1994) prepared quantum dot nanocomposites consisting of CdSe nanoparticles embedded in ZnSe thin films, which is a larger band gap semiconductor. The semiconductor matrix was expected to stabilize the quantum dots and protect them against oxidation. The CdSe nanoparticles were brought in the aerosol phase by using the electrospray method. The aerosol was transported into an organometallic CVD reactor where the ZnSe film was being deposited. It was observed that the optical properties of these quantum dots were preserved during this process. Another kind of nanocomposite quantum dot was synthesized by Salata *et al.* (1994a), who imbedded PbS nanoparticles in a polymer film. An aerosol of a liquid containing $Pb(NO_3)_2$ and a polymer precursor was obtained by an electrospray system and then reacted with H_2S from the gas phase producing PbS nanoparticles. The PbS nanoparticles covered with a polymer layer were then driven by the electrical field towards the substrate. The optical absorption spectrum showed a large blue shift, corresponding to a theoretical mean particle diameter of 4.6 nm. Using a $Cd(NO_3)_2$ solution, CdS nanoparticles were also obtained with an average diameter smaller than 5 nm claimed to have a narrow size distribution (Salata *et al.*, 1994b).

5.2 Synthesis of luminescent nanocrystalline silicon

Littau *et al.* (1993) synthesized Si nanoparticles with sizes between 3 and 8 nm by pyrolysis of 3-30 ppm Si_2H_6 at 865 °C in a furnace flow reactor operated at 1.4 bar He. The aerosol was then diluted with He and reacted with O_2 in a second furnace at

700°C, yielding a passivating layer of SiO_2. The shell thickness of the nanoparticles was 1.2 nm. The aerosol was collected as colloid in ethylene glycol and size-selected using a liquid phase method. The luminescence of the colloid obtained was weak but could be improved through chemical treatment to reach a quantum yield of 5 % at room temperature and 50 % quantum yield below 50 K (Wilson *et al*., 1993). The luminescence shifted to higher energy with decreasing particle size, indicating thereby quantum confinement effects (Brus *et al*., 1995).

Both Kanemitsu *et al.* (1993) and Kawaguchi and Miyazima (1993) decomposited SiH_4 with a Nd:YAG laser at 10-20 mbar and obtained Si nanoparticles with sizes between 3 and 20 nm. The samples were oxidized at room temperatures for several weeks in a clean air box, resulting in a thin amorphous SiO_2 layer around the particles. These particles exhibited a strong visible photoluminescence at room temperature, the maximum-intensity wavelength being however independent of the Si core size. Takagi *et al.* (1990) applied a microwave plasma to decompose SiH_4. The diameter of the Si nanocrystals could be varied in this case from 2.5 to 20 nm. They were blown through a transfer pipe onto a substrate in a vacuum chamber and oxidized. Here, the luminescence peak showed a weak dependence on the particle diameter. Saunders *et al.* (1993) produced 2 - 4 nm sized Si crystallites by a spark source. Immediately after synthesis, the sample consisting of a 10 nm thick particulate film showed little or no visible photoluminescence. After exposure to air however, the luminescence increased dramatically. Werwa *et al.* (1994) used pulsed laser ablation combined with supersonic expansion and obtained 2-3 nm Si nanoparticles, which then showed visible photoluminescence after surface passivation by chemical means. More detailed studies (Seraphin *et al*., 1996) showed that the maximum-intensity wavelength is determined by the particle size, while the luminescence intensity is determined by the degree of surface passivation.

The first report on size classification in the gas phase originates from Camata *et al.* (1996). They obtained Si nanoparticles with a high-voltage electric spark discharge in an inert gas at atmospheric pressure and then size-selected them by a DMA. The nanoparticles, with sizes selected between 2.8 and 11 nm, were collected on a substrate by an electrostatic precipitator or hypersonic impactor. The standard deviation of the classified aerosol was 1.2 - 1.3. The size distribution of the smallest particles selected, i.e., 2.8 nm, showed however also the presence of a significant amount of larger particles. This was due to the omission of the neutralizer at this size resulting in multiply charged particles.

5.3 Fabrication of gas sensors

Ogawa *et al*. (1981a, b) produced a thick film consisting of SnO_2 nanoparticles with mean sizes between 3 and 15 nm. A heated boat containing Sn was placed underneath an RF-induced plasma in a low-pressure O_2 gas. The SnO_2 nanoparticles were deposited on a substrate placed above the O_2 plasma. The macrostructure of the films, which ranged from porous columnar to spongy, was found to be dependent on the O_2 pressure. The porous columnar structure had the highest selectivities, and was used to detect water, ethanol and isobutane vapor. A similar reactive plasma system was used by Zhu *et al.* (1993), who replaced the RF coil by the more economic d.c. gas discharge ring electrode. The nanoparticles in the film had a mean size of 40 nm and exhibited a good sensitivity to ethanol vapor.

The results obtained by Ogawa will be analyzed here more in detail, as they provide a good insight in the mechanisms of gas sensing. A 10 -50 µm thick porous film composed of 15 nm SnO_2 particles showed a high gas sensitivity and an improved gas selectivity in comparison to sensors consisting of micron-size grains (Ogawa *et al.*, 1981b). From mobility measurement results it was postulated that due to the small dimensions of the conduction channels in the nanoparticles the depletion layer has a large influence on the conductivity (Ogawa *et al.*, 1982).

Gas sensors based on semiconducting metaloxides are applied for the detection of explosive or toxic gases. The measurement signal bases on the conductivity, σ, of the material. In the temperature range normally used (400-700 K) the chemical sensing mechanism is a result of a surface reaction between chemically adsorbed oxygen and reducing gases. The oxygen is chemically adsorbed in the form of O_2^-, O^- or O^{2-} and induces a depletion zone at the surface which has a lower conductivity in comparison with the bulk because electrons are bounded to the adsorbed oxygen. A reducing gas will reduce the concentration of chemically adsorbed oxygen so that the conductivity increases. Chemical reactions at the surface were investigated by means of mass-spectrometric measurements of the desorption products when the film is heated (Kohl, 1989). The following reaction was found when ethanol reacts with O^- at the surface of SnO_2:

$$C_2H_5OH + O^- \leftrightarrow CH_3CHO + H_2O + e \qquad (5.1)$$

The adsorbed C_2H_5OH molecules oxidize at 250°C to CH_3CHO. The electron which is freed by this reaction effectively increases the conductivity of the SnO_2.

Gas sensors based on ultrafine thin films of metal oxides are known since several decades. A porous film composed of particles with diameters between 6 and 20

nm showed an improved sensitivity and a high gas selectivity due to the increased surface area to volume ratio (Ogawa *et al.*, 1981b). The increased sensitivity was investigated by means of Hall measurements (Ogawa *et al.*, 1982). Contrary to the simple measurement of the conductivity σ , which is equal to the product $qn\mu_H$, allow these to measure separately the concentration of carriers, n, and the mobility, μ_H. The charge number on the carrier is indicated by q.

The carrier concentration n was found to change with gas concentration. It was shown that for normal thin films the mobility μ_H was independent of the gas concentration but that the thin films composed of nanoparticles showed a strong dependence of the gas concentration (Fig. 5.1). This is the reason for the increased sensitivity of these films.

The largest effects were found for the films with the smallest particles. The changed mobility can be understood by the following schematic model visualized in Fig.5.2. Fig 5.2a shows several SnO_2 nanoparticles before C_2H_5OH is adsorbed. The O^- species which are chemisorbed at the surface act as scattering centers and hinder the movement of the charge carriers. The area where this hindering occurs is given by the Debye length L_D:

$$L_D = \left(\frac{\varepsilon k_B T}{q^2 n} \right)^{1/2} \qquad (5.2)$$

where ε is the dielectric constant, k_B is Boltzmann constant T is the absolute temperature. When the size of the particles approaches that of the Debye length, a clear decrease in the mobility of the charge carriers results. The adsorption of ethanol results in the decrease or elimination of these scattering centers, as can be seen in Fig 5.2b. This effective increase in the size of the conduction channel leads to an increase in the mobility. The Debye length for the ultrafine particle films was found to be around 3 nm. Other investigations showed also a large increase in sensitivity when the particle size drops below 10 nm (Xu *et al.*, 1991). But also film thickness, stoichiometry and morphology of the film have influence on the electrical properties of the film (Sanjines *et al.*, 1990).

The combined effects of particle size distribution, the nature of the contacts between the particles and the chemical composition of the surface are so complex that the production of semiconducting oxide gas sensors is at present mainly an empirical technology. Grain size control and size homogeneity remain hence a fundamental issue of investigation (Dieguez *et al.*, 1996).

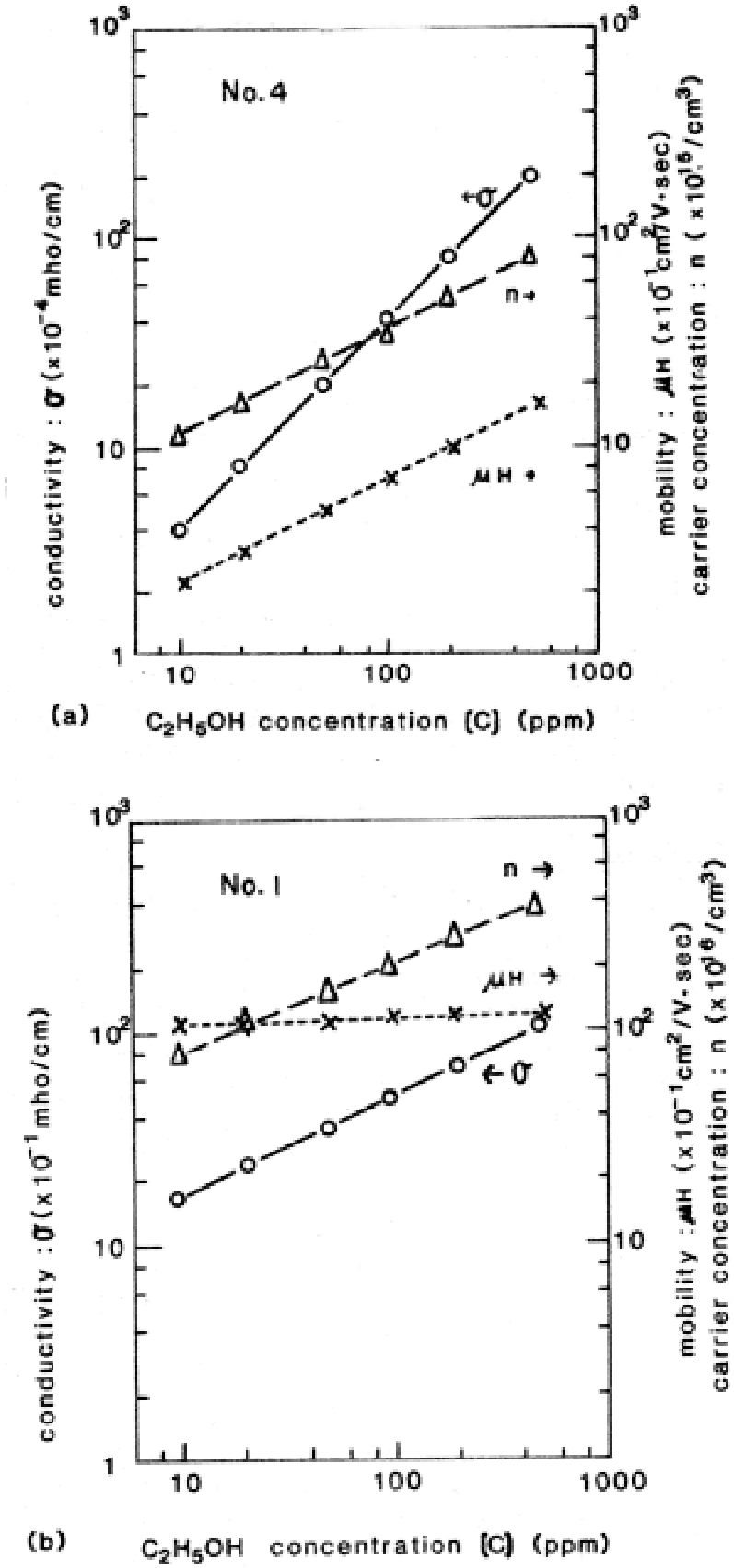

Fig. 5.1. Hall measurements for nanoparticle film (a) and thin film (b) (from Ogawa et al., 1982)

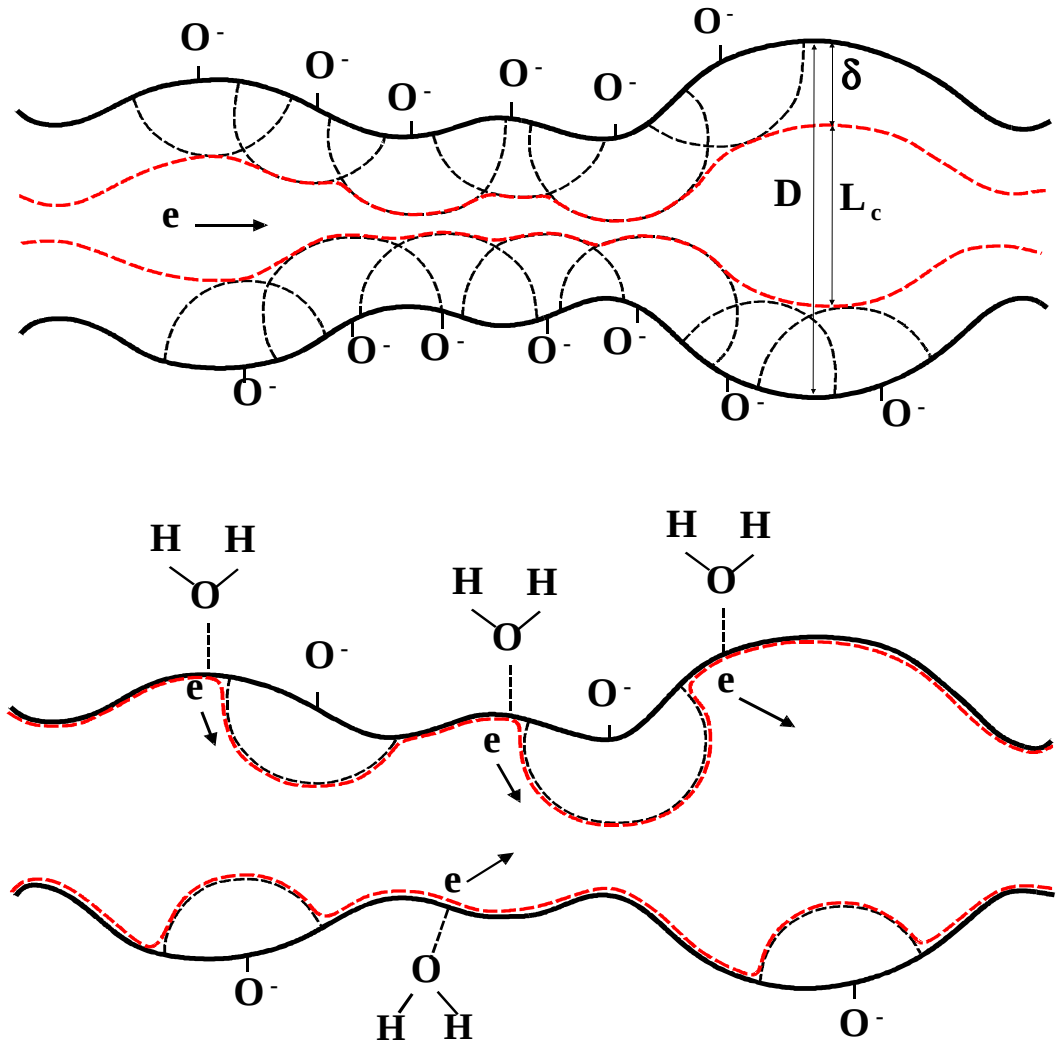

Fig. 5.2. Schematic model for the modification of the conductivity channel by gas adsorption a) before gas adsorption and b) after gas adsorption (from Ogawa et al, 1982)

Adachi *et al.* (1988) applied an evaporation-reaction type aerosol generator to produce SnO_2 particles. Sn was vaporized in a furnace and reacted with O_2, yielding upon cooling SnO_2 particles with mean sizes between 10 and 100 nm. The particle size distribution was measured using a DMA-CNC combination. Thin nanoparticle films on a glass substrate were produced by accelerating the particles through a critical orifice into a low-pressure chamber. The electrical properties of the films were sensitive to H_2 especially at room temperature.

Spray pyrolysis of a $SnSO_4$ solution yielded a SnO_2 powder consisting of 1 µm sized agglomerates composed from nanocrystals of 9 nm mean size. This is a result of multiple nucleation in the drying aerosol droplet. The powder was sintered at several temperatures, which led to a slight increase in the size of the nanocrystals. The resulting sensor characteristics for ethanol and CO vapor were measured. It appears that the electrical resistance was mainly due to the contacts between the agglomerates (Schmatz *et al*., 1994). A Sn-precursor, dibutyltindiacetate, in a solution was spray-pyrolysed unto a heated substrate by using a ultra-high frequency nebulizer. This led to a polycrystalline SnO_2 film with crystallite sizes between 8 and 25 nm. When a Pt-precursor, platinumacetylacetonate, was added to the solution, 3-5 nm sized Pt nanoparticles were dispersed on the SnO_2 grains (Labeau *et al.*, 1993). A similar procedure was adopted to produce SnO_2 sensors doped up to 10 vol% with Pd nanoparticles, showing an increased sensitivity for CO and ethanol vapor (Gautheron *et al.*, 1993).

The inert gas condensation method has also been used for synthesis of gas-sensing materials. Volkening *et al.* (1995) produced Pd nanoparticles with a size of 10 - 15 nm using inert gas condensation with a DC/RF magnetron sputter source. The gas-sensing properties of the compacted powder for H_2 gas were analyzed using a contactless method. Lin *et al.* (1995) produced a thin film gas sensor by depositing TiO_2 nanoparticles on a thin film of TiO_2 to obtain good adherence. The nanoparticles were synthesized by evaporation of Ti in a low-pressure mixture of O_2 and He. By carefully heating the film, a porous structure was obtained showing a good sensitivity for H_2S gas. In order to increase the sensitivity further, a dopant in the form of Pt nanoparticles with sizes less than 10 nm was added on top of the nanocrystalline film. This increased the sensitivity and decreased the operating temperature by some 200°C below that of a regular TiO_2-based gas sensor.

Hu *et al.* (1997) applied reactive laser ablation in order to produce very thin granular SnO_2 films. An excimer laser with a wavelength of 248 nm and pulse width of 20-30 ns at 3 Hz repetition rate ablated a rotating Sn target. Nanoparticles were deposited on a substrate heated above the melting point of Sn and placed several centimeters below the target. Although the ablation was carried out at a pressure of 1 mbar O_2, the oxidation of Sn nanoparticles took place mainly on the substrate. TEM micrographs and X-ray diffraction showed grain sizes of 10-30 nm. The thinnest films produced were 24 nm and showed a high sensitivity to ethanol vapor.

5.4 Fabrication of conducting films

Lee *et al.* (1996) applied a RF plasma reactor operating at atmospheric pressure to produce thin ITO films based on nanoparticles. A precursor solution containing $SnCl_4$ and $In(NO_3)_3$ was ultrasonically nebulized and introduced into the plasma region. The film on the substrate located underneath the plasma consisted of particles with sizes between 50 and 150 nm and was optically transparent. The resistivity was found too high for practical applications except for using these films in transparent electrical heaters. Zhao and Pan (1994) obtained ZnO nanoparticle films by evaporating Zn in a dc arc jet using O_2 as the plasma forming gas in a low pressure environment (0.1-10 mbar). The optical properties of the films which were composed of particles with mean sizes between 20 and 80 nm showed a transmission between 20 and 80 % in the visible spectrum. The IR spectra showed size effects and the electrical properties were found to depend on the amount of O_2 absorption.

5.5 Synthesis of high-temperature superconductors (HTS)

Aerosols have been used extensively in the preparation of HTS films, but mainly as a means of transport of the precursors to the reaction zone where they evaporate (Wang *et al.*, 1990, Salazar *et al.*, 1992). The HTS material can also be produced as a powder, which can be sintered into larger HTS units. This has been done mainly by spray pyrolysis yielding particles in the size range of 0.1-5 µm. Okuyama *et al.* (1993) obtained particles of about 50 nm of a bismuth oxide superconductor ($Bi_2CaSr_2Cu_2O_x$) by evaporating volatile organometallic precursors and reacting the gas mixture of the different precursors with O_2 in a furnace reactor. The particles were then collected with an electrostatic precipitator. The presence of the 80 K phase was found by X-ray diffraction, and it was shown that a precise control of the reactor temperature and residence time could avoid the undesirable formation of the 10 K phase.

Chadda *et al.* (1991) obtained an $YBa_2Cu_3O_{7-y}$ /CuO composite powder consisting of 25-50 nm crystallites by spray pyrolysis of a nitrate solution. This powder could be converted into $YBa_2Cu_4O_8$ by heating it in an O_2 atmosphere. However, this conversion was not successful when using a larger grained powder of 100-250 nm. $YBa_2Cu_4O_8$ has certain advantages over $YBa_2Cu_3O_{7-y}$ with respect to the flux pinning requirement, see section 2.7. Takao *et al.* (1996) used an electrostatic aerosol mixing process to produce composite $BaZrO_3/YBa_2Cu_3O_{7-y}$ particles. Here, after a separate synthesis of the two compounds the $BaZrO_3$ aerosol particles smaller than 100 nm were electropositively charged while the $YBa_2Cu_3O_{7-y}$ particles with a

size of 500 nm were electronegatively charged. By imparting a multiple charge to the superconducting particles and singly charging the nanoparticles, a coating of $BaZrO_3$ nanoparticles on the $YBa_2Cu_3O_{7-y}$ particles resulted after mixing. After sintering the powder to a superconducting composite body, the critical current density increased by a factor of ten as compared to the same superconducting material without $BaZrO_3$ nanoparticles.

5.6 Synthesis of magnetic materials

Inert gas evaporation using a low-pressure, between 1 and 10 mbar, is used routinely to produce magnetic nanoparticles for research purposes. It stems from the pioneering work in the group of Uyeda who produced Fe, Co and Ni particles from 8 to 200 nm by evaporating the metal in low-pressure Ar (Tasaki *et al.* ,1965). As an example of a more recent work, Gangopadhyay *et al.* (1992) evaporated Fe from a heated crucible and obtained nanoparticles on a cooled substrate by thermophoresis. The Fe nanoparticles with sizes between 5 and 20 nm were subjected to a slow oxidation in a Ar-air mixture to passivate the surface. The resulting Fe-oxides layers were 1-2 nm thick. The highest coercivity at room temperature was 1050 Oe for nanoparticles with a diameter of 13 nm. Particles smaller than 9 nm were superparamagnetic.

Alloy nanoparticles have also been obtained using inert gas evaporation. They have magnetic properties of technological importance when composed of a magnetic material imbedded in a nonmagnetic material. Li *et al.* (1994) obtained by evaporating the alloy in Ar gas FeCr particles having mean sizes between 8 and 36 nm. Some Fe and Fe-oxide was also detected in the particles, making the interpretation of the magnetic properties difficult.

A method better suited for large scale synthesis is inert gas condensation. Balachandran *et al.* (1995) evaporated Cr in low pressure He and collected the Cr nanoparticles on a cold finger. The powder could be compacted in-situ after an oxidation step with O_2 to form Cr_2O_3. The nanophase powder with a mean particle size of 10 nm exhibited superparamagnetic behavior. Sintering led to an increase in particle size, up to 80 nm at the highest sintering temperature, with the superparamagnetic properties partly retained.

Pyrolysis in a oxyhydrogen flame of $Fe(CO)_5$ or iron acetylacetonate dissolved in toluene led to γ-Fe_2O_3 powders with particle sizes as small as 5 nm (Grimm *et al.*, 1997). Laser pyrolysis of $Fe(CO)_5$ using a pulsed CO_2 laser has been applied by Majima *et al.* (1994), who obtained nanoparticles with a mean size of 13 nm. The particles contained a large percentage of γ-Fe which is normally stable at high

temperatures and which is paramagnetic up to room temperatures. Vollath *et al.* (1995) synthesized γ-Fe_2O_3 particles in the size range 4-5 nm by heating $FeCl_3$ in a microwave plasma. The particles were found to be superparamagnetic. A superparamagnetic nanocomposite was synthesized by Zachariah *et al.* (1995), who used a CH_4/O_2 flame as the reaction environment to which Fe and Si-bearing precursors such as $Fe(CO)_5$ and $SiO_2(CH_3)_6$, were added. The magnetic Fe_2O_3 nanoparticles of 5-10 nm were encapsulated in SiO_2 particles ranging from 30 to 100 nm. The samples showed evidence for superparamagnetism over a wide temperature range. Hwang *et al.* (1997) synthesized 18 nm Ni nanoparticles encapsulated by a graphite layer several nanometers thick, to protect them against oxidation. This was done by an arc discharge plasma in a He environment with Ni contained in a graphite anode. The encapsulated Ni nanocrystals showed a significant lowering of the magnetic coercivity and saturation magnetization , as compared with bulk Ni.

Spray pyrolysis has been used to produce nanoparticles of magnetic materials such as ferrites and garnets. Tang *et al.* (1989) atomized a solution of $Fe(NO_3)_3$ and $Ba(NO_3)_2$ in water, and obtained after pyrolysis in a furnace spherical particles of $BaFe_{12}O_{19}$ with sizes between 40 and 80 nm. Post-annealing was necessary to obtain a crystalline phase and achieve high coercivity values, up to 5360 Oe at room temperature.

Mizuguchi *et al.* (1994) introduced aqueous metal nitrate solutions in aerosol form into an ICP and obtained $BaFe_{12}O_{19}$ nanoparticles with sizes between 10 and 50 nm. Film formation, obtained by an electrostatic precipitator at elevated temperatures using a H_2-O_2 flame, proved problematic due to deviations from stoichiometry. De Marco *et al.*(1993) used a R.F. plasma suited for large scale nanoparticle production. $Ni_{0.5}Zn_{0.5}Fe_2O_4$ and $NiFe_2O_4$ nanoparticles with a mean size of about 55 nm were produced, containing Fe_3O_4 as an impurity. The nanoparticle powders had higher coercivities than the bulk material.

5.7 Conclusions: special process requirements for selected functional applications

Two chemical compounds are selected for the remaining of this work. One component is selected for its potential quantum confinement effects. PbS is a narrow-gap IV-VI semiconductor with a cubic rock salt structure and is an attractive candidate for the study of quantum confinement effects as its hole Bohr radius is 9 nm. This results in strong confinement effects as compared to the II-VI semiconductors such as CdS and CdSe with Bohr radii of about 1 nm (Machol *et al.,* 1994). The confinement results in a blue shift in the optical absorption spectrum (Brus, 1984). The other

material, SnO_2, is selected for its gas-sensing properties, which were described extensively in Chapter 5.3.

A size uniformity is important in order to study or make use of quantum size effects, as a distribution of particle sizes will decrease or smear out these effects. In view of the high specific surface and activity of SnO_2 nanoparticles, considerable improvement in sensing properties is expected. In order to understand the relationship between gas-sensing behaviour and particle size better it is necessary to generate monodisperse nanoparticles, because a distribution of particle sizes will decrease the special properties and complicates the interpretation of the experimental results. This was also emphasized by Göpel and Schierbaum (1995) in their review article on future prospects of SnO_2 gas sensors: 'Particular emphasis is put on preparing thin films of SnO_2 with homogeneous particle sizes in the nanometre range'. At the moment no gas sensors based on almost equal-sized nanoparticles are available. As shown in the preceding chapter, Brownian coagulation rules out the synthesis of monosized particles by gas-phase synthesis. Therefore, a size-fractionation technique will be applied in this work in which a narrow fraction is taken from the original wide distribution.

Apart from the size homogeneity, the chemical composition is important. In case of PbS, it should be investigated if it is possible to retain the stoichiometry when sublimating the source material directly. Furthermore, the particles should be crystalline as amorphous material does not show semiconducting properties. In case of the SnO_2, some deviation of stoichiometry is desirable, as in substoichiometric SnO_2, denoted by SnO_x, the electrical transport properties are more suitable for gas sensing applications. Furthermore, some special handling techniques are necessary. The nanoparticles have to be brought onto a suitable substrate for use in functional applications. For some applications, e.g. doped gas sensors, a control over the mixing of two different nanoparticle flows is needed. It will be shown in the next chapter that the use of electrical effects allows size-fractionation, nanoparticle deposition and controlled mixing.